

# PALEOSTRIPv1.0 - a user-friendly 3D backtracking software to reconstruct paleo-bathymetries

Florence Colleoni<sup>1</sup>, Laura De Santis<sup>1</sup>, Enrico Pochini<sup>1,2</sup>, Edy Forlin<sup>1</sup>, Riccardo Geletti<sup>1</sup>,  
Giuseppe Brancatelli<sup>1</sup>, Magdala Tesauro<sup>2,3</sup>, Martina Buseti<sup>1</sup>, and Carla Braitenberg<sup>2</sup>

<sup>1</sup>National Institute for Oceanography and Applied Geophysics - OGS. Borgo Grotta Gigante 42/c, 34010 Sgonico (TS), Italy

<sup>2</sup>University of Trieste, Department of Mathematics and Geoscience, Trieste, Italy

<sup>3</sup>University of Utrecht, Department of Geosciences, the Netherlands

**Correspondence:** Florence Colleoni (fcolleoni@inogs.it)

**Abstract.** Paleo-bathymetric reconstructions provide boundary conditions to numerical models of ice-sheet evolution and ocean circulation, critical to understanding their evolution through time. The geological community lacks of a complex open-source tool that allows for community implementations and can strengthen research synergies. To fill this gap, we present PALEOSTRIPv1.0, a MATLAB open-source software designed to perform 1D, 2D and 3D backtracking of paleo-bathymetries.

- 5 PALEOSTRIP comes with a Graphical User Interface (GUI) to facilitate computation of sensitivity tests and to allow the users to switch on and off all the different processes and thus separate the various aspects of backtracking. As such, all physical parameters can be modified from the GUI. It includes 3D flexural isostasy, 1D thermal subsidence and possibilities to correct for prescribed sea level and dynamical topography changes. In the following we detail the physics embedded within PALEOSTRIP and we show a few applications on a drilling site (1D), a transect (2D) and a map (3D), taking the Ross Sea (Antarctica) as a
- 10 case study. PALEOSTRIP has been designed to be modular and to allow users to insert their own implementations.

*Copyright statement.* TEXT

## 1 Introduction

- On-going climate changes are urging the scientific community to project climate future evolution in response to carbon emissions trajectories (e.g. the Shared Socio-economical Pathways by Riahi et al., 2017). The Coupled Model Intercomparison
- 15 Project (CMIP), now ending phase 6 (Eyring et al., 2016), has been producing a large amount of climate projections until 2100. However some of the climatic variables, for example, the deep ocean, the carbon cycle and the ice sheets and glaciers, react more slowly to climate changes (e.g. Colleoni et al., 2018b; Noble et al., 2020), although showing evidence of changes over the past decades already (Caesar et al., 2021). Their main response has yet to be observed and is likely to happen beyond the 21st century, which is encouraging climatologists to project changes on longer timescales of few centuries to millennia (e.g.
- 20 IPCC, 2013, 2019). Projecting to such timescales implies to design corresponding, realistic carbon emission trajectories and so far, millennial scale emissions trajectories are just extension of existing emission scenarios beyond 2100 (e.g. Golledge et al.,

2015; DeConto and Pollard, 2016). At this point, the exercise becomes difficult and this is when reconstructing past climates becomes important. It allows to test the response of the Earth's climate under different, but realistic, atmospheric greenhouse gas concentrations (GHGs) (e.g. Haywood et al., 2019). GHGs higher than present-day or future ones, i.e. larger than 400 ppm for atmospheric CO<sub>2</sub>, can only be found for times older than 3 million years ago (e.g. Zhang et al., 2013; Bracegirdle et al., 2019). Going back to those times, or even before, it is likely that the tectonic setting responsible for other boundary conditions, such as oceanic gateways, elevation of mountain ranges, continental margin expansion, as well as the location and extent of continental masses themselves, differed from that of the present-day (e.g. Herold et al., 2008; Frigola et al., 2018; Müller et al., 2018a; Straume et al., 2020; Hochmuth et al., 2020). Nevertheless, simulating and reconstructing past climatic conditions can bring useful hints on how future climate might evolve and also help narrowing the range of likely long-term carbon emissions trajectories.

Reconstructing past topographies and bathymetries is fundamental for paleoclimate and paleo ice sheet simulations (e.g. Otto-Bliesner et al., 2017; Colleoni et al., 2018a; Straume et al., 2020; Paxman et al., 2020). The numerous oceanic deep drilling campaigns that occurred over the past decades have the potential to constrain such reconstructions, but not when part of the information has been eroded and/or reworked during geological time by other tectonic or climatic processes. In addition, during sediment deposition, the bathymetry itself changes due to different processes, such as the loading of accumulated sediments, thermal subsidence acting on extended continental crust, subsidence/uplift induced by mantle dynamics (dynamic topography) or sea level changes (e.g. Kirschner et al., 2010; Celerier, 1988; Sclater and Christie, 1980). Other external factors also influence the bathymetry, as for example ice loading in polar areas. By accounting for all those factors and processes, by decompacting and removing overlying sediments, it is possible to backtrack the bathymetry, and thus the paleo-water depth, of a chosen specific time interval. Conversely, if the target of the study is to reconstruct the burial history of a sedimentary basin, the technique is the same, but needs constraints on the paleo-water depths and is called "Backstripping" (Steckler and Watts, 1978).

There are a few existing open-source backstripping or backtracking codes. Flex-Decomp by Badley Geoscience Ltd. (Kusznir et al., 1995) allows to perform 2D-flexural backstripping or backtracking and its code is not open-source. A 3D version of Flex-Decomp exists but is not open-source (Roberts et al., 2003) and is used exclusively by Badley Geoscience Ltd., and not available externally. It comes along with the sister program Stretch by Badley Geoscience Ltd., a software to compute forward modeling of basin evolution that provides spatially variable stretching factors cross-section to be used by Flex-Decomp. BasinVis (Lee et al., 2016, 2020) is a MATLAB open-source code with a graphical user interface. It calculates compaction trends from input drill sites (1D) lithological units. The estimated compaction trends can be applied in thickness restoration of stratigraphic units and subsidence analysis data that can be spatially interpolated between input drill sites to reconstruct a temporal basin evolution. Dressel et al. (2015, 2017) perform 3D backtracking southwestern African continental margin accounting for 1D-thermal subsidence and Pratt isostasy, taking into account lateral density variations. PyBacktrack, is a 1D-backtracking and backstripping open-source code (Müller et al., 2018b) aimed at reconstructing paleo-bathymetries. It allows to process drilling sites both on oceanic and continental crust and can be connected to the suite of geodynamical open-source software GPlates (<https://www.gplates.org/>) and benefits from geodynamical corrections related to kinematic, tectonic and geodynamic

models of plates tectonic movements through time. DeCompactionTool (Hölzel et al., 2008) propose a similar approach than pybacktrack, for 1D well, but allows to perform a Monte-Carlo like analysis, i.e., perform a large number of 1D runs based on a possible range of main physical parameters defined by admissible minimum and maximum values, to provide a quantitative estimate on the backstripping error.

3D flexural backstripping and backtracking are needed to reconstruct basin-wide or continental-wide areas that will be prescribed as boundary conditions within climate and ice sheet models. A few studies mentioned the use of 3D backstripping (e.g. Scheck et al., 2003; Hansen et al., 2007; Smallwood, 2009; Amadori et al., 2017), and a very limited number provides with 3D flexural backstripping (Roberts et al., 2003; Steinberg et al., 2018; Roberts et al., 2019).

Here we present PALEOSTRIP, a MATLAB open-source software designed to perform 1D, 2D and 3D backtracking of paleobathymetries. PALEOSTRIP comes with a Graphical User Interface (GUI) to facilitate computation of sensitivity tests and allows the users to switch all the different processes on and off and thus separate the various aspects of backtracking. As such, all physical parameters can be modified from the GUI. It includes 3D flexural isostasy, 1D thermal subsidence and possibilities to correct for prescribed sea level and dynamical topography changes. In the following we detail the physics embedded within PALEOSTRIP and show a few applications on a drilling site (1D), a transect (2D) and a map (3D), taking the Ross Sea (Antarctica) as a case study.

## 2 Model Framework and requirements

PALEOSTRIP is a MATLAB open-source code developed under the GNU General Public License v3.0. It is composed of a set of routines called by a graphical interface from which users can load data, change physical parameters, plot and save results (Fig. 1). The code is distributed on Github (<https://github.com/flocolleoni/PALEOSTRIPv1.0>) along with a User Manual providing all necessary explanations and examples on how to input data and use PALEOSTRIP functionalities. **Note that the final version related to this study has been corrected with minors bugs and the main “Plot & Save” graphical interface has been modified to implement 12 color scales, among which, 9 color-blind friendly scales from Crameri et al. (2020). We thus invite the readers to download again the code from Github and from Zenodo.**

PALEOSTRIP has been designed and coded with MATLAB (R2019b) and run on any operating system. Most of the code should be compatible with previous versions of MATLAB, provided that it includes the App Designer toolbox. The code is incompatible with GUIDE and from MATLAB R2020, GUIDE is not available anymore. PALEOSTRIP cannot be run without its graphical interface, thus a version of MATLAB with the App Designer toolbox is necessary.

### 2.1 PALEOSTRIP Graphical User Interface

PALEOSTRIP Graphical User interface (GUI) is composed of two different tabs. The first one is dedicated to input data, physical parameters and choices of physical methods for each of the processes accounted for in backtracking (Fig. 1). The second one is dedicated to plotting backtracked data and saving results (see Sect. 6). The GUI can be launched either through the MATLAB main interface and by double clicking on the corresponding App Designer GUI file, or by exporting it as a stand-alone

application that can be executed without opening MATLAB. We do not provide a built-in PALEOSTRIP application, since the  
90 compilation of the applications depends on the operating system on which it is created, but we provide the PALEOSTRIP code  
instead. As such, the user is free to export it from the App Designer tool.

## **2.2 Format of input and output data**

### **2.2.1 Coordinate system**

Cartesian coordinates (in meters) are required to perform flexural isostasy calculations, as the flexural response depends on  
95 the distance from the load. Consequently, input data must be provided on a cartesian coordinates grid. PALEOSTRIP does  
not run on geographical coordinates and does not provide any tool to convert input data from geographical to cartesian coor-  
dinates. However, many open-source softwares or codes exist to perform this step, such as the MATLAB Mapping Toolbox  
(<https://it.mathworks.com/products/mapping.html>), The Generic Mapping Tools 6 (<https://www.generic-mapping-tools.org/>),  
OBLIMAP2 (Reerink et al., 2016) or any other GIS software.

### **2.2.2 Input files**

Horizon depths have to be provided individually in single ASCII files, defining the given quantity along with its coordinates.  
For example: horizon depth Z for a 1D drill site; extension along the transect and depth (X, Z) for 2D transects; the horizontal  
position (X,Y) and depth (Z) for 3D horizon maps. Output data are saved with the same format. PALEOSTRIP does not  
read and write grids in the NetCDF format. Lithological parameters must be provided in a separate ASCII file and are spatially  
105 uniform. In the present study, the input data files associated to each case studies are zipped in paleostrip\_examples.zip, available  
on GitHub at (<https://github.com/flocolleoni/PALEOSTRIPv1.0>). Since the lithological parameters varies substantially given  
the composition of sediments and their depositional context, we refer the reader to Kominz et al. (2011) for values and detailed  
explanations on how to retrieve the decompaction coefficients for the different lithologies of marine sediments.

## **3 PALEOSTRIP: backtracking and limitations**

110 During its evolution, a submarine continental margin can experience various processes that modify its morphology. For ex-  
ample, a rifted basin can form in response to plate tectonics displacement and/or erosion that shapes the basic structure of  
the margin. Surface erosion from the hinterland can supply the margin with sediments filling morphological depressions if the  
accommodation space is large enough. The accommodation space depends on initial conditions, on the tectonic and on the  
thermal subsidence of the continental margin, i.e., the lithosphere and asthenosphere cooling during and after the rifting lead-  
115 ing to a deepening of the margin through time. Eustatic and regional sea level changes modulate the available accommodation  
space and the distance from the sediment sources. To reconstruct the past subsidence history of a continental margin at a given  
time, all those processes have to be accounted for and corrected in a procedure called "Backstripping" (Steckler and Watts,  
1978). Backstripping consists in decompacting and removing sediment layers iteratively back in time to reconstruct the past



tectonic subsidence history of a basin or a margin (Fig. 2):

$$Z(i) = \frac{\rho_m - \rho_s}{\rho_m - \rho_w} S(i) + WD(i) - \frac{\rho_m}{\rho_m - \rho_w} \Delta SL(i) \quad (1)$$

where the first term of the right-hand side corresponds to the isostatic compensation ( $\rho_s$  sediment density,  $\rho_m$  mantle density,  $\rho_w$  seawater density) of the  $i$ th sediment layer thickness  $S(i)$  accumulated on the basement,  $WD(i)$  is the paleo-water depth of the  $i$ th layer and the last term of the equation corresponds to the water-load correction due to sea level variations ( $\Delta SL$ ) at time of the  $i$ th layer. This equation solves the time-evolution of total subsidence  $Z(i)$  of the basement and  $WD$  needs to be provided for each  $i$  layer to solve the equation. Conversely, in case the focus is on reconstructing time-varying paleo-water depths  $WD(i)$ , the procedure is called "Backtracking" and a total subsidence  $Z(i)$  time-evolution needs to be provided as input to the equation:

$$WD(i) = Z(i) - \frac{\rho_m - \rho_s}{\rho_m - \rho_w} S(i) + \frac{\rho_m}{\rho_m + \rho_w} \Delta SL(i) \quad (2)$$

PALEOSTRIP is a backtracking software and is designed to reconstruct paleo-water depths given a provided subsidence history. Equations above are the original backstripping and backtracking equations developed by Steckler and Watts (1978) and explained therein in major detail. Over the past decades, it has also been found that mantle convection generates changes in the regional topography, the so-called "dynamic topography" (Müller et al., 2018a). Paleo-water depth needs to be corrected for dynamic topography changes  $\Delta DynT(i)$  causing uplift or subsidence of the topography and bathymetry:

$$WD(i) = Z(i) - \frac{\rho_m - \rho_s}{\rho_m - \rho_w} S(i) + \frac{\rho_m}{\rho_m + \rho_w} \Delta SL(i) + \Delta DynT(i) \quad (3)$$

In this equation, the second and third terms in the right-hand side have been written accounting for Airy local isostatic compensation. However PALEOSTRIP also makes use of 2D and 3D flexural isostasy (See Sect. 3.2). In this case, the second and third terms in the right-hand side of the equation represent the depth correction due to flexural response to unloading of sediment during backtracking and to water loading/unloading due to sea level changes.

In the following, we explain how each term of Eq. (3) is treated within PALEOSTRIP. Most of the equations reported below are taken from Allen and Allen (2013) if not otherwise specified. The various aspects of the backtracking procedure are explained following PALEOSTRIP workflow (Fig. 3).

Note that the physics implemented does not allow the treatment of oceanic crust in this version. This can be done by adding a few more options in the GUI mainly for thermal subsidence (e.g. Müller et al., 2018b). This can be easily implemented.

### 3.1 Decompaction

The total sediment thickness  $S$  accumulated at a given time can be obtained by reconstructing its compaction history. Eroded sediments that are transported to the margin deposit and accumulate wherever the accommodation space allows for it. Accumulated sediments compact through time under loading, for example, by overlying sediments. Therefore, to reconstruct the paleo-architecture of a continental margin at a given time, the sediment layers of a margin are stripped off sequentially, and

the remaining underlying sediments need to be gradually decompacted. Decompaction is thus central to backstripping and  
150 backtracking.

Compaction or decompaction of sediments both imply a change in total volume  $V_{total}$  of deposited sediments mostly caused by changes in the porosity of sediments and to a lesser extent by sediment compression. In submarine environments sediments are saturated by water and their compaction implies the decrease in pore fluid pressure by expelling the water out of the sediment layers. Conversely, decompaction involves an increase in the pore fluid pressure by injecting water within the  
155 compacted sediments. The decompaction process consists in calculating the changes in porosity of the various sediment layers to determine the amount of water that was contained in the sediments at the time of their deposition, based on their lithology. The depth of the decompacted sediment layers is recalculated on the basis of those porosity changes. Laboratory experiments have determined that for large depths, the evolution of porosity can be described by an exponential relationship rather than by a linear empirical equation:

$$160 \quad \phi = \phi_0 e^{-cz} \quad (4)$$

where  $\phi_0$  corresponds to deposition porosity at the seafloor (or at surface if emerged),  $c$  is the exponential slope decay coefficient (also referred as compaction coefficient herein) depending on the lithology expressed in  $1/km$  and  $z$  is depth in km. This empirical equation implies that  $\phi_0$  is decreased by the factor of  $1/e$  at the depth of  $1/c$  km.

In general, the mass of the total sediment column at a given time does not change: in submarine environment the water that  
165 is expelled from the sediments is implicitly added to the water column above the underlying sediments during the compaction processes. Thus, only the volume of the sediment layers  $V_{total}$  changes due to volume water changes  $V_w$ , which allows to integrate the porosity equation (4). Considering a unit cross-sectional area, the thickness of water  $W_T$  to be added to the compacted sediment volume, in order to decompact it is given by:

$$W_T = \int_{z_i}^{z_{i+1}} \phi_0 e^{-cz} dz \quad (5)$$

170 which on integration gives:

$$W_T(i) = \frac{\phi_0}{c} \{e^{-cz'_i} - e^{-cz'_{i+1}}\} \quad (6)$$

where  $z'_i$  and  $z'_{i+1}$  are the newly decompacted depths of  $z_i$  and  $z_{i+1}$ . Because the volume of sediment grains  $V_{sed}$  remains unchanged, the integrated compacted sediment thickness  $S_{dt}$  between two given depths, considering a unit cross-sectional area, can be written as:

$$175 \quad S_{dt} = z_{i+1} - z_i - \frac{\phi_0}{c} \{e^{-cz_i} - e^{-cz_{i+1}}\} \quad (7)$$

Based on the fact that  $V_{total} = V_{sed} + V_w$ , the decompacted depths  $z'(i)$  for a unit cross-sectional area can be inferred and the final decompaction equation is given by:

$$z'_{i+1} - z'_i = z_{i+1} - z_i - \frac{\phi_0}{c} \{e^{-cz_i} - e^{-cz_{i+1}}\} + \frac{\phi_0}{c} \{e^{-cz'_i} - e^{-cz'_{i+1}}\} \quad (8)$$

PALEOSTRIP solves this equation iteratively (starting with  $z'_i = 0$  and then for the next iterations) until convergence is reached.

180 Lithological parameters, i.e. the decompaction coefficient  $c$  and the depositional surface porosity  $\phi_0$  are prescribed in the user-provided parameter files (See Sect. 6).

### 3.2 Isostatic correction

Sediments load the basement of the continental margin and cause a local and regional subsidence during accumulation. Water also loads the basement due to eustatic sea level variations, leading to changes in the water depth  $WD$ , also caused by ocean  
185 bottom subsidence and/or uplift through time. In addition, during the decompaction, the newly computed decompacted depths of the remaining sediment layers need to be adjusted to account for the changes of their porosity and thus their density due to the presence of water filling the pores. For each sediment layer, the porosity  $\rho_{ds}(i)$  of the decompacted thickness  $S_d(i)$  of the  $i - th$  sediment layer is:

$$\phi_{ds}(i) = \frac{\phi_0}{c} \frac{e^{-cz'(i+1)} - e^{-cz'(i)}}{S_d(i)}; \quad (9)$$

190 and the decompacted sediment bulk density  $\rho_{ds}(i)$  of the  $i - th$  sediment layer is given by:

$$\rho_{ds}(i) = \phi_{ds}(i)\rho_w + (1 - \phi_{ds}(i))\rho_s(i) \quad (10)$$

At each timestep, the removal of the top layer causes the decompaction of the underlying sediment layers. Removed sediment layers are substituted with seawater. Unloading causes an isostatic compensation that can be calculated by means of different isostatic methods. In PALEOSTRIP, two methods are implemented.

#### 195 3.2.1 Airy local compensation

The Airy local compensation is the most used isostatic method in backstripping and backtracking. It involves a local depth compensation  $Z_{airy}(i)$  for which the rocks/sediments and the underlying asthenosphere are considered to be in hydrostatic equilibrium:

$$Z_{airy}(i) = S_d(i) \left( \frac{\rho_m - \rho_{ds}(i)}{\rho_m - \rho_w} \right) \quad (11)$$

200 This method implies that the weight of the sediments in a given grid point does not impact on the adjacent points. Therefore, in the case of a 2D transect or a 3D map, grid points are independent from each others. This is of course not realistic and the Airy local compensation should be applied preferably to the decompaction of wells only (Roberts et al., 1998).

#### 3.2.2 Flexural compensation

When considering a wider area, i.e. decompacting a 2D transect or a 3D basin, a flexural compensation is required because  
205 a surface load tends to influence its surroundings. An Airy local compensation would not capture this effect and thus would

overestimate the isostatic correction to be applied during the backstripping or backtracking (Roberts et al., 1998). Flexural compensation is based on the flexural strength of the lithosphere that is defined by its flexural rigidity  $D$  (in N m):

$$D = \frac{ET_e^3}{12(1 - \nu^2)} \quad (12)$$

where  $E$  corresponds to the Young Modulus (N/m<sup>2</sup>),  $T_e$  is the effective elastic thickness of the lithosphere (m) and  $\nu$  is the Poisson ratio. Total 1D-flexure of the lithosphere for a line load on an infinite plate is given by the general analytical solution (Turcotte and Schubert, 2002):

$$D \frac{d^4 w}{dx^4} + (\rho_m - \rho_w)gw = q \quad (13)$$

and its 2D expression:

$$D \nabla^4 w(x) = D \frac{d^4 w}{dx^4} + D \frac{d^4 w}{dy^4} + 2 - D \frac{d^4 w}{dx^2 dy^2} + (\rho_m - \rho_w)gw(x) = q \quad (14)$$

where  $w$  is the deflection of the lithosphere (m),  $g$  is the gravity acceleration (m/s<sup>2</sup>),  $q(x, y)$  is the vertical load (N/m<sup>2</sup>) applied to the lithosphere and  $x$  and  $y$  are the coordinates in the horizontal plane. In this equation, downward deflected lithosphere is substituted with seawater  $\rho_w$ . The load  $q(x, y)$  (in N/m<sup>2</sup>) associated to each  $i$ -th sediment layer is calculated as:

$$q(i) = \rho_{ds}(i)gS_d(i) \quad (15)$$

In PALEOSTRIP, 2D and 3D finite difference versions of Eq. (13) and Eq. (14) have been implemented (e.g. Equation 9 and 10 in Wickert, 2016). They are based on Chapman (2015) `flex2d` and Cardozo (2009) `flex3dv` MATLAB codes that have been adapted to PALEOSTRIP needs. `flex3dv` routine is available at <http://www.ux.uis.no/%7Enestor/Public> and `flex2d` is available at <https://www.jaychapman.org/matlab-programs.html>. By means of a finite difference scheme, flexure can be computed by mean of an analytical solution (e.g. `gfex`, Wickert, 2016) whereas other numerical methods use the superposition of local solutions to point loads in the wavenumber domain (e.g. Green's functions, TAFI v1.0, Jha et al., 2017), or in the spectral domain (Wienecke et al., 2007), for example. These use biharmonic equation for plate flexure with uniform elastic properties. Approaches using the convolution method also allow to use spatially variable elastic properties (e.g. Braitenberg et al., 2003, 2002). A file of spatially variable  $T_e$  can be provided through the GUI (Fig. 1a, bottom). A spatially uniform  $T_e$  can also be prescribed directly from the GUI. All other parameters involved in the flexural or Airy isostasy can be modified from the GUI (density constants, Poisson Ratio and Young Modulus).

### 3.3 Thermal subsidence

Thermal subsidence corresponds to a vertical contraction of the lithosphere. During a rifting phase, in a first step, the lithosphere stretches apart and thins, which causes a net increase in heat outflow towards the surface due to the upwelling of the underlying asthenosphere. The stretching is generally not uniform, but reconstructions of past stretching process require knowledge about

235 plate tectonics strain rate (e.g. Müller et al., 2019) which is beyond the scope of our software. The first step is called "initial" subsidence. In a second step, the "thermal subsidence", the stretched lithosphere constricts due to cooling. To account for those effects during backstripping, PALEOSTRIP adopts the 1D-thermal subsidence model from McKenzie (1978) that assumes an instantaneous stretching (syn-rift) and a single rifting phase. The initial subsidence  $Z_{init}$  is given by:

$$Z_{init} = \frac{T_{IL} \left[ (\rho_m - \rho_c) \frac{T_{IC}}{T_{IL}} \left( 1 - \frac{\alpha_v T_m T_{IC}}{2 T_{IL}} \right) - \frac{\rho_m \alpha_v T_m}{2} \right] \left( 1 - \frac{1}{\beta} \right)}{\rho_m (1 - \alpha_v T_a) - \rho_w} \quad (16)$$

240 where  $T_{IL}$  and  $T_{IC}$  are the initial lithospheric and crustal thicknesses at the beginning of rifting,  $\beta$  is the stretching factor,  $\alpha_v$  is the coefficient of thermal expansion,  $\rho_c$  is the crustal density,  $\rho_m$  is the mantle density. In this equation, the subsidence is isostatically compensated by water ( $\rho_w$ ) using the Airy local compensation. This 1D instantaneous model can be improved by adopting a time-evolving approach to the extension, such as for example Jarvis and McKenzie (1980). However, comparison between Jarvis and McKenzie (1980) and McKenzie (1978) revealed that the two models show no or only little discrepancy if  
 245 the duration of extension, given the time required to extend by a factor  $\beta$ , is about  $60/\beta^2$  Ma if  $\beta \leq 2$  or  $60(1 - 1/\beta)^2$  Ma if  $\beta \geq 2$  (Jarvis and McKenzie, 1980). During the second step, the thermal subsidence occurs after the end of rifting (post-rift) and accounts for the vertical thermal conduction which takes the shape of an exponential function decaying with time:

$$Z_{thermal}(t) = E_0 \frac{\beta}{\pi} \sin\left(\frac{\pi}{\beta}\right) \left( 1 - \exp\left(-\frac{t}{\tau}\right) \right) \quad (17)$$

where  $t$  corresponds to the time elapsed since the end of rifting expressed in seconds (example: time of backtracked horizon =  
 250 14 Ma; time since the end of rifting = 76 Ma;  $t = (76 - 14) * 3600 * 24 * 365 * 10^6$  ).

$$E_0 = \frac{4\rho_m \alpha_v T_m T_{IL}}{\pi^2 (\rho_m - \rho_w)}, \text{ and } \tau = \frac{T_{IL}^2}{\pi^2 \kappa} \quad (18)$$

where  $\kappa$  is the thermal diffusivity. The total thermal subsidence is given by:

$$Z_{tot\_thermal} = Z_{init} + Z_{thermal} \quad (19)$$

In PALEOSTRIP, during the backtracking procedure, paleo-water depths are corrected by removing the increment of thermal  
 255 subsidence between each timestep and present-day. This is because backtracking is an iterative process departing from a known state, i.e. present-day. Because  $Z_{init}$  is constant in time, it cancels out, and the thermal subsidence correction is given by:

$$\Delta Z_{tot\_thermal}(t) = (Z_{init} + Z_{thermal}(t)) - (Z_{init} + Z_{thermal}(0)) \quad (20)$$

and thus,

$$\Delta Z_{tot\_thermal}(t) = Z_{thermal}(t) - Z_{thermal}(0) \quad (21)$$

260 where  $t$  varies from present to past in this equation following backstripping procedure, i.e.,  $t$  is an age older than present-day (0).  $\Delta Z_{tot\_thermal}$  is thus positive with  $Z_{thermal}$  being larger for younger times, i.e. larger time elapsed since the end of rifting.

Note that by applying the 1D model from McKenzie (1978) to 2D transects and 3D maps, it is assumed that no horizontal heat advection occurs. From the GUI tab interface (Fig. 1b), almost all parameters involved in the thermal subsidence can be modified (Age of end of rifting,  $T_{IL}$  and  $T_{IC}$ ,  $\alpha_v$ ,  $\kappa$ ). The stretching factor  $\beta$ , can be formulated through several methods:

- 265 (1) prescribe a constant and uniform  $\beta$  factor that will be used at each timestep of backtracking to calculate the thermal subsidence.
- (2) linearly interpolate (in the x direction for 3D maps) between two prescribed constant and uniform stretching factors,  $\beta_1$  and  $\beta_2$
- 270 (3) input a user-based constant but spatially variable  $\beta$  factor, in one direction (x grid), to compute spatially variable thermal subsidence for a 2D transect or input a 2D (x,y grid) file to compute spatially variable thermal subsidence for 3D maps.

### 3.4 Sea Level correction

On long timescales, sea level has been varying with time due to plate tectonics changing the dimensions of ocean basins (e.g. Müller et al., 2018a) and, on shorter timescales, due to continental ice storage within ice sheets, ice caps and glaciers during cold periods, as for example during the second half of the Cenozoic (last 34 Ma, e.g. Miller et al., 2020). Classically, only eustatic sea level changes have been considered for correcting the subsidence or the paleo-water depth. For the last 34 Ma, eustatic sea level is usually defined relatively to the present-day total ocean area ( $362.15 \cdot 10^6 \text{ km}^2$ ) because it is assumed that this area evolved only a little and not enough to significantly alter this number. For time periods older than that, eustatic sea level changes have to be expressed according to the ocean area of the time. Considering only eustatic sea level changes is highly approximated ice sheets growth and decay, leading to sea level variations of growing amplitude over the past 34 Ma

275 citep[e.g.][Miller2020]. The variations induced by glaciations have much shorter timescales, i.e.  $10^4 - 10^5$  yrs, compared with those induced by plate tectonics ( $10^5 - 10^6$  yrs). Associated sea level changes are not spatially uniform and induce changes in the Earth's gravity field (e.g. Tamisiea et al., 2001) and regional self-gravitating sea level changes can substantially vary from eustasy (e.g. Tamisiea et al., 2001; Clark et al., 2002; Milne and Mitrovica, 2008).

In PALEOSTRIP sea level ( $SL$ , in m) is corrected as for the thermal subsidence:

$$285 \quad \Delta SL(t) = SL(t) - SL(0) \quad (22)$$

where  $t$  varies from present to past in this equation following backtracking procedure, i.e.,  $t$  is an age older than present-day(0).  $\Delta SL$  is expressed relative to present and it can therefore assume positive or negative values, i.e. induce an uplift or a subsidence. Most of the sea level variations timeseries found in literature already correspond to variations relative to present, i.e., already are in the form of Eq. 22. Thus in order to avoid confusion for the user, three different ways of correcting water depth with sea

290 level changes have been implemented within PALEOSTRIP and can be managed through the GUI (Fig. 1c):

- (1) prescribing constant and uniform sea level correction  $\Delta SL$  applied at each timestep of the backtracking (ex: correction at a time where sea level is lower by 100 meters relative to present is prescribed as  $-100$  in the GUI);
- (2) applying a spatially uniform but time-varying sea level correction based on timeseries from Haq et al. (1987) or from Miller et al. (2020) (implemented within PALEOSTRIP);

295 (3) applying a user-provided timeseries or a constant in time but spatially varying map (x,y, z) of sea level changes relative to present.

The last option allows to prescribe sea level changes calculated with Glacio-Isostatic Adjustment models (e.g. SELEN<sup>4</sup> Spada and Melini, 2019) to account for regional self-gravitating effects of ice sheets growth and decay.  $\Delta SL$  is used to compute the water-load correction to adjust the water depth  $WD$ . In Eq. 3 water load due to sea level change is described based on Airy  
300 local compensation. In PALEOSTRIP, the water-load due to sea level change is computed using the isostatic method previously selected to carry out decompaction (see Sect. 3.2). Note that if isostasy is deactivated, no water-load correction is computed.

### 3.5 Dynamic topography

Mantle dynamics generate flows that cause time-varying surface topography and bathymetry deformations, which are called “dynamic topography”. The timescale at which the mantle flow produces dynamic topography which occurs at long wavelength  
305 ( $\approx 5\,000$  to  $10\,000$  km Hoggard et al., 2016). The current mantle- driven dynamic topography was revealed by estimating the residual topography, obtained after removing the isostatic topography, generated by thickness and density contrasts within the lithosphere the isostatic effect of the lithosphere calculated using seismic data compilations (e.g. Flament et al., 2013; Hoggard et al., 2016). Continental margins stratigraphic observations revealed that the dynamic topography evolves quickly with time, thus potentially impacting on long-term climate evolution (Hoggard et al., 2016). Austermann et al. (2017) showed that the  
310 magnitude of past interglacial sea level proxies partly results from dynamic topography and suggested correcting sea level proxies before inferring the relative contribution of past ice sheet to the sea level changes at that time. Furthermore, simulated Pliocene dynamic topography changes accounted for in Antarctic ice sheet simulations revealed that ice sheet stability is highly influenced by mantle dynamics that create or cancel pinning areas at the surface (Austermann et al., 2015). Thus past reconstructions of continental morphology and shallow margins should account for past evolution of dynamic topography.  
315 Müller et al. (2018a) recently provided timeslices of reconstructed dynamic topography over the past 240 Ma, which constitutes a strong basis to calculate a dynamic topography correction.

PALEOSTRIP provides three ways to correct for dynamic topography changes through its GUI (Fig. 1d):

- (1) prescribing a uniform and constant dynamic topography change relative to present-day that will be applied to each timestep of the backtracking procedure;
- 320 (2) using a user-based spatially uniform timeseries of dynamic topography changes relative to present;
- (3) using user-based 2D maps of dynamic topography changes relative to present, e.g. Müller et al. (2018a); Note that Müller et al. (2018a) is not implemented within PALEOSTRIP. Maps of dynamic topography are inputs to PALEOSTRIP and the user is free to use any reconstructions. Note that inputs of dynamic topography require some pre-processing to be adjusted to the area of interest before being passed through the GUI.

325 The correction is calculated as for sea level changes (Eq. 22):

$$\Delta DynT(t) = DynT(t) - DynT(0) \quad (23)$$

where  $t$  varies from present to past in this equation following backstripping procedure, i.e.,  $t$  is an age older than present (0).  $\Delta DynT$  is expressed relative to present, and since dynamic topography is not spatially uniform at global level, it can therefore assume positive or negative values, i.e. induce an uplift or a subsidence.

### 330 3.6 Sediment erosion

Sediment erosion and depositions are the main processes involved in the building of continental margins. Present-day identified sedimentary units that may not reflect the real number of sedimentary units at a given time in the past because meanwhile, some of the layers might have been eroded. Erosion is identified within sediment cores as hiatus and as high amplitude, sometimes truncational reflectors within marine seismic profiles. During backstripping, one should move back eroded sediments to their  
335 presumed original locations (e.g. Paxman et al., 2019), which can be either within the backstripped area or outside the backstripped area. If eroded sediments are moved back in the backstripped area, then the total number of layers should be modified during the backward modeling process. The current version of PALEOSTRIP does not treat erosion and does not allow to vary the total number of sedimentary layers once input at the beginning of the procedure. A good description of how to handle erosion during backstripping is provided in Chapter 5.4 of Wangen (2010).

## 340 4 PALEOSTRIP Grid interpolation

PALEOSTRIP handles 1D data (drill sites), 2D data (transects) and 3D data (grids). All calculations, except flexure, are performed on the grid or array of original input data. For 2D and 3D data, all input horizon depths have, however, to be on the same grid/array (identical coordinates), and spacing along the X and Y directions must be constant. For 3D grids, spacing in the X direction can differ from spacing in the Y direction. For example, 2D transects must have horizons depths of the same  
345 length. 3D maps can be provided as an irregular polygon and all horizon depths must be provided on the same exact polygon (see examples in Sect. 6). At last, grid spacing  $dx$  and  $dy$  must be integers (e.g.  $dx=10$  km and not  $dx=4.3$  km).

### 4.1 2D data: vertical transects

Vertical transect imply that input data are provided along an horizontal direction X and a vertical direction (depth) Z. For the need of flexure calculation, the original sediment loads array is extended (duplication of last values at both edges) to about  
350 90 % of its length from both edges (Fig. 4a). The sediment loads are then placed at the center of an expanded domain (three times larger than original array length) to avoid edge effects on flexure correction. After flexure calculation, the correction is extracted and relocated on the original array domain. All the other backtracking calculations occur on the original input array. Note that spatially variable lithospheric elastic thickness is also interpolated and extrapolated following this procedure.

### 4.2 3D data: maps

355 Maps implies that data are provided along the two horizontal directions X and Y and along the vertical direction Z. Input data are read as scattered data, and not as gridded data. This means that points are unstructured and are not written in a file



following a classical NX\*NY structure but treated as independent single points. When data is treated as scattered, this takes more computational time, but this also allows one to input either structured gridded data, or irregular polygon data. This facilitates all computations and avoids unnecessary duplication of routines for 1D, 2D or 3D cases. For the need of flexure, 3D data are interpolated (preserving their original horizontal resolution) on a regular rectangular grid. The original input grid is expanded (extrapolation of the last values from the edges) to about 30% from all sides of the grid. The sediment loads are then placed at the center of an expanded domain (twice larger than original grid dimension) to avoid edge effects on flexure correction (Fig. 4b). After flexure calculation, the correction is extracted and relocated on the original grid domain. All the other backtracking calculations occur on the original input grid. Note that spatially variable lithospheric elastic thickness is also interpolated and extrapolated following this procedure.

5 PALEOSTRIP validation

We backtrack a 2D transect with PALEOSTRIP and with Flex-Decomp (Kusznir et al., 1995) to validate the results. The transect used in the case study is a revised version of the one studied by De Santis et al. (1999), the BGR80-007 seismic profile. The transect BGR80-007 is composed of 9 identified seismic stratigraphic unconformities. The transect is about 250 km long, broadly oriented North-South and is located in the Eastern Ross Sea (Fig. 5). The set of initial data is composed of ten files: the actual bathymetry of the Ross Sea, present-day depth of the nine seismic unconformities including present-day depth of the basement below (Fig. 6a). Depths are related to present regional sea level.

The eleventh file contains the lithological parameters of the layers to be decompacted, as well as other parameters needed by PALEOSTRIP, excluding present-day bathymetry: LAYER is the layer number (1 to N, from bottom to top); POROSITY is the deposition porosity (unitless), DEC CON (1/KM) corresponds to the porosity decompaction coefficient, MAT DEN (KG/M3) corresponds to the compacted sediment density; AGE BASE (Million years ago, Ma) is the age of horizons at the base of the layers and NAME is the string name of horizons. The parameters are taken from the study of De Santis et al. (1999) and the lithological parameter file follows this format:

NUMBER OF LAYERS =	9				
LAYER	POROSITY	DEC CON	MAT DEN	AGE BASE	NAME
		(1/KM)	(KG / M3)	(MA)	
1	0.4900	0.2700	2680.00	95.00	basement
2	0.4500	0.4500	2680.00	26.00	rsu_6
3	0.4500	0.4500	2680.00	24.90	rsu_5b
4	0.4500	0.4500	2680.00	19.70	rsu_5a
5	0.4500	0.4500	2680.00	18.00	rsu_5
6	0.4500	0.4500	2680.00	14.20	rsu_4

390	7	0.4500	0.4500	2680.00	10.00	rsu_3
	8	0.4500	0.4500	2680.00	4.00	rsu_2
	9	0.4500	0.4500	2680.00	0.60	rsu_1

To facilitates the comparison, thermal subsidence, sea level and dynamic topography are switched off both in PALEOSTRIP and in Flex-Dedcomp. We compare the final backtracked depths of the basement using Airy local isostasy and flexural isostasy with different lithospheric elastic thicknesses (Fig. 6b). The match between PALEOSTRIP and Flex-Decomp is very good and persistent discrepancies (a few tens to a hundred of meters) are likely due to (1) the different ways of computing flexural isostasy, in the spectral domain for Flex-Decomp and with finite difference for PALEOSTRIP and (2) to re-interpolation of the load to a different resolution in Flex-Decomp (no reinterpolation in PALEOSTRIP) and (3) to different extrapolation of the load outside of the original transect length to avoid edge effect on flexure. In PALEOSTRIP, the last point of the transects at both edges is duplicated to extend the original length of about 80% at both sides (Fig. 4a). We also compare PALEOSTRIP backtracked results with those using the analytic solution from TAFI v1.0 (Jha et al., 2017) and implemented within PALEOSTRIP for the need of comparison (Fig. 6c). Similarly to the comparison with Flex-Decomp, we only account for isostasy and the other processes are switched off. Re-interpolation of the loads is performed by PALEOSTRIP in both cases. Comparison between PALEOSTRIP (finite difference scheme) and TAFI v1.0 reveal almost identical results.

405 Finally, we test the isostasy and thermal subsidence model by comparing those obtained by PALEOSTRIP and Flex-Decomp. De Santis et al. (1999) originally used Flex-Decomp with  $\beta=2$ , with the age of rifting set to 85 Ma and various lithospheric elastic thickness values to restore paleobathymetries. We use the same parameters on this revised transect both in Flex-Decomp and in PALEOSTRIP. Match between PALEOSTRIP and Flex-Decomp is very good (Fig. 6d).

## 6 Case study: example of the Ross Sea

410 PALEOSTRIP GUI presents a Plot & Save interface to support each steps of backtracking: the user can plot initial input data, backtracked data, calculated intermediate variables relevant to the backtracking process and save them to ASCII files (Fig. 7). The user can also extract some 2D transects or 1D wells from 3D backtracked maps or 2D transects, plot and save them to ASCII files. In the following, we provide two case studies to illustrate the possibilities of PALEOSTRIP. Note that the physical parameters, sea level correction or thermal subsidence related variables are not tuned since the aim of the examples is to illustrate the physics of PALEOSTRIP rather than to provide a realistic reconstruction of the paleo-bathymetries of this area.

Both the cases are taken from the continental margin in the Western Pacific Sector of Antarctica, in the Ross Sea (Fig. 5). Sediment layers mostly accumulated after the main rifting phases that occurred in this area between 95 and 79 Ma (Stock and Cande, 2002; Decesari et al., 2007; Siddoway et al., 2004). **Ross Sea stratigraphic data are currently being revised and differ from ANTOSTRAT data (Brancolini et al., 1995)** on which the following 3D example is based. New reconstructed Ross Sea paleo-bathymetry using revised data will be the object of a specific contribution. ANTOSTRAT data have been recently used in pan-Antarctic reconstructions of past topographies and bathymetries (Paxman et al., 2019; Hochmuth et al., 2020).

6.1 Well (1D): Deep Sea Drilling Project DSDP site 273 - Ross Sea

In the last example, we decompact the drilling site DSDP273 Hayes and Frakes (1975) from the Western Ross Sea (Fig. 5). It has two main identified seismic unconformities above the basement. Lithological parameters are taken from De Santis et al. (1999) and the lithological parameters file (see Sect. 5) is:

NUMBER OF LAYERS =						3
LAYER POROSITY DEC CON MAT DEN AGE BASE NAME						
						(1/KM) (KG / MC) (MA)
1	0.4500	0.2700	2680.00	95.00	basamento	
2	0.4500	0.4500	2680.00	21.00	rsu_5	
3	0.4500	0.4500	2680.00	19.00	rsu_4a	

Backtracking is performed using Airy local isostasy since flexure cannot be applied to 1D drilling sites. We also add thermal subsidence in order to illustrate the difference in backtracked depths of those unconformities (Fig. 8). The layout of Fig. 8 is not the layout of PALEOSTRIP but results have been assembled to highlight the impact of thermal subsidence on backtracked depths. As for 2D transects, all intermediate variables and input conditions can be plotted and saved.

6.2 Map (3D): ANTOSTRAT data

In this example we backtrack the depth of the Mid-Miocene unconformity ( 14 Ma) across the Ross Sea from ANTOSTRAT atlas (Brancolini et al., 1995). The initial grid is an irregular polygon. The set of initial data is composed of three files: the actual bathymetry of the Ross Sea, present-day depth of Mid-Miocene unconformity and presumed present-day depth of the basement below (Fig. 9).

The fifth file contains the lithological parameters of the layers to be decompact (see Sect. 5) and are taken from De Santis et al. (1999) and the lithological parameters file is:

NUMBER OF LAYERS =						2
LAYER POROSITY DEC CON MAT DEN AGE BASE NAME						
						( % ) (1/KM) (KG / CC) (MA)
1	0.450	0.450	2680.0	95.000	Basement	
2	0.450	0.450	2680.0	14.200	RSU4	

PALEOSTRIP is run several times to add one component at once amongst, isostasy, thermal subsidence, sea level correction and dynamic topography correction. Thanks to this approach, the user can perform ensembles of simulations to retrieve

455 sound statistics about the model parameter space. Two series are shown, one using Airy isostatic correction (Fig. 10), and the other using flexural isostatic correction (Fig. 11). Paleo-bathymetry retrieved with flexural isostasy produces a quite different morphology from the one computed using Airy isostasy, as already observed by Roberts et al. (1998). Sea level and dynamic topography (Fig. A1b) corrections are not big enough to produce a significant change of the overall morphology. However, they matter for the bathymetric highs, and especially, the shallowest one, as few tens of meters can uplift those highs above  
460 sea level. PALEOSTRIP allows the user to plot different variables amongst initial input data and computed quantities, such as isopach, density, porosity or isostatic correction, so the user can check and separate the various processes to perform a detailed analysis of their impact on the paleo-bathymetric reconstruction (Fig. A1).

## 7 Conclusions

PALEOSTRIP is one of the first open-source 3D backtracking software. It can process paleo-bathymetries for 1D drilling  
465 sites, 2D transects and 3D maps. It allows to separate the various processes involved in the backtracking procedure. Thanks to this approach, the user can perform ensembles of simulations to retrieve sound statistics about the model parameter space. PALEOSTRIP has been designed to be modular, to allow users to insert their own modifications. The code is documented and implementation of new modules would only require minor work.

*Code and data availability.* The version of the code and example data used in this manuscript are available on Zenodo <http://doi.org/10.5281/zenodo.50928>  
470 or on github <https://github.com/flocolleoni/PALEOSTRIPv1.0>.

## Appendix A: Case studies: settings

### A1 Table of Physical parameters

In all the examples provided, we used PALEOSTRIP default values automatically inserted within GUI (Table 1).

### A2 PALEOSTRIP workflow

### 475 A3 Backtracked intermediate variables

Here we plot some of the intermediate physical variables calculated during the backtracking procedure and available for plotting through PALEOSTRIP GUI: sediment isopachs, decompacted density, decompacted porosity, isostatic correction and dynamic topography (Fig. A1). Thermal subsidence is also available for plotting but since here we employ a spatially uniform  $\beta$  value, thermal subsidence is consequently spatially uniform over the domain and thus we do not display it.

480 *Author contributions.* F.C. developed PALEOSTRIP code. L.D.S. and R.G. provided input data for the case studies. All the authors contributed to discussions about numerical developments of PALEOSTRIP and writing of the manuscript.

*Competing interests.* The authors declare no competing interests.

*Acknowledgements.* This work is supported by the PNRA national Italian projects: PNRA18\_00002, “Onset of Antarctic Ice Sheet Vulnerability to Oceanic conditions (ANTIPODE)” PNRA16\_00016, “West Antarctic Ice Sheet History from Slope Processes–Eastern Ross Sea (WHISPERS)” and by the MAE bilateral Italy-US project US16GR04, “Global Sea Level rise & Antarctic Ice Sheet Stability predictions: guessing future by learning from past(GLSAISS)”.  
485

## References

- Allen, P. A. and Allen, J. R.: Basin Analysis: Principles and Applications, 2nd Edition I , Wiley, 2 edn., 2013.
- Amadori, C., Toscani, G., Di Giulio, A., García-Castellanos, D., Fantoni, R., Ghielmi, M., et al.: Restoration of Paleo-Shorelines Through  
 490 Lithospheric 3D Modeling and Backstripping Analysis: The Example of the Po Plain-Northern Adriatic Region During Late Messinian  
 Sea-Level Drop, in: Offshore Mediterranean Conference and Exhibition, Offshore Mediterranean Conference, 2017.
- Arndt, J. E., Schenke, H. W., Jakobsson, M., Nitsche, F. O., Buys, G., Goleby, B., Rebesco, M., Bohoyo, F., Hong, J., Black, J., et al.: The  
 International Bathymetric Chart of the Southern Ocean (IBCSO) Version 1.0—A new bathymetric compilation covering circum-Antarctic  
 waters, *Geophysical Research Letters*, 40, 3111–3117, 2013.
- 495 Austermann, J., Pollard, D., Mitrovica, J. X., Moucha, R., Forte, A. M., DeConto, R. M., Rowley, D. B., and Raymo, M. E.: The impact of  
 dynamic topography change on Antarctic ice sheet stability during the mid-Pliocene warm period, *Geology*, 43, 927–930, 2015.
- Austermann, J., Mitrovica, J. X., Huybers, P., and Rovere, A.: Detection of a dynamic topography signal in last interglacial sea-level records,  
*Science Advances*, 3, e1700457, 2017.
- Bracegirdle, T. J., Colleoni, F., Abram, N. J., Bertler, N. A., Dixon, D. A., England, M., Favier, V., Fogwill, C. J., Fyfe, J. C., Goodwin,  
 500 I., et al.: Back to the future: Using long-term observational and paleo-proxy reconstructions to improve model projections of Antarctic  
 climate, *Geosciences*, 9, 255, 2019.
- Braitenberg, C., Ebbing, J., and Götze, H.-J.: Inverse modelling of elastic thickness by convolution method—the Eastern Alps as a case  
 example, *Earth and Planetary Science Letters*, 202, 387–404, 2002.
- Braitenberg, C., Wang, Y., Fang, J., and Hsu, H.: Spatial variations of flexure parameters over the Tibet–Qinghai plateau, *Earth and Planetary*  
 505 *Science Letters*, 205, 211–224, 2003.
- Brancolini, G., Buseti, M., Marchetti, A., De Santis, L., Zanolla, C., and Cooper, A. K. e. a.: Seismic stratigraphic atlas of the Ross Sea,  
 Antarctica., in: *Geology and seismic stratigraphy of the Antarctic margin*, Antarctic Research series, edited by Cooper, A. K., Barker, P.,  
 and G., B., vol. 68, pp. 271–286, 1995.
- Caesar, L., McCarthy, G., Thornalley, D., Cahill, N., and Rahmstorf, S.: Current Atlantic Meridional Overturning Circulation weakest in last  
 510 millennium, *Nature Geoscience*, pp. 1–3, 2021.
- Cardozo, N.: flex3dv ©MATLAB software - <http://www.ux.uis.no/%7Enestor/Public/flex3dv.zip>, 2009.
- Celerier, B.: Paleobathymetry and geodynamic models for subsidence, *Palaios*, 3, 454–463, 1988.
- Chapman, J.: flex2d ©MATLAB software - <https://www.jaychapman.org/matlab-programs.html>, 2015.
- Chen, B., Haeger, C., Kaban, M. K., and Petrunin, A. G.: Variations of the effective elastic thickness reveal tectonic fragmentation of the  
 515 Antarctic lithosphere, *Tectonophysics*, 746, 412–424, 2018.
- Clark, P. U., Mitrovica, J., Milne, G., and Tamisiea, M.: Sea-level fingerprinting as a direct test for the source of global meltwater pulse 1A,  
*Science*, 295, 2438–2441, 2002.
- Colleoni, F., De Santis, L., Montoli, E., Olivo, E., Sorlien, C. C., Bart, P. J., Gasson, E. G., Bergamasco, A., Sauli, C., Wardell, N., et al.: Past  
 continental shelf evolution increased Antarctic ice sheet sensitivity to climatic conditions, *Scientific reports*, 8, 1–12, 2018a.
- 520 Colleoni, F., De Santis, L., Siddoway, C. S., Bergamasco, A., Golledge, N. R., Lohmann, G., Passchier, S., and Siegert, M. J.: Spatio-temporal  
 variability of processes across Antarctic ice-bed–ocean interfaces, *Nature Communications*, 9, 1–14, 2018b.
- Cramer, F., Shephard, G., and Heron, P.: The misuse of colour in science communication, *Nature Communication*, 11, 5444,  
<https://doi.org/https://doi.org/10.1038/s41467-020-19160-7>, 2020.

De Santis, L., Prato, S., Brancolini, G., Lovo, M., and Torelli, L.: The Eastern Ross Sea continental shelf during the Cenozoic: implications  
525 for the West Antarctic ice sheet development, *Global and Planetary Change*, 23, 173–196, 1999.

Decesari, R., D.S. Wilson, D., Luyendyk, B., and M., F.: Cretaceous and Tertiary extension throughout the Ross Sea, Antarctica, in *Antarctica: A Keystone in a Changing World*, in: Online Proceedings of the 0th ISAES, edited by Cooper, A. and et al., C. R., p. 6, ISAES, 2007.

DeConto, R. M. and Pollard, D.: Contribution of Antarctica to past and future sea-level rise, *Nature*, 531, 591–597, 2016.

Dressel, I., Scheck-Wenderoth, M., Cacace, M., Lewerenz, B., Götze, H.-J., and Reichert, C.: Reconstruction of the southwestern African  
530 continental margin by backward modeling, *Marine and Petroleum Geology*, 67, 544–555, 2015.

Dressel, I., Scheck-Wenderoth, M., and Cacace, M.: Backward modelling of the subsidence evolution of the Colorado Basin, offshore Argentina and its relation to the evolution of the conjugate Orange Basin, offshore SW Africa, *Tectonophysics*, 716, 168–181, 2017.

Eyring, V., Bony, S., Meehl, G. A., Senior, C. A., Stevens, B., Stouffer, R. J., and Taylor, K. E.: Overview of the Coupled Model Intercomparison Project Phase 6 (CMIP6) experimental design and organization, *Geoscientific Model Development*, 9, 1937–1958,  
535 <https://doi.org/10.5194/gmd-9-1937-2016>, 2016.

Flament, N., Gurnis, M., and Müller, R. D.: A review of observations and models of dynamic topography, *Lithosphere*, 5, 189–210, 2013.

Frigola, A., Prange, M., and Schulz, M.: Boundary conditions for the middle Miocene climate transition (MMCT v1. 0), *Geoscientific Model Development*, 11, 1607–1626, 2018.

Golledge, N. R., Kowalewski, D. E., Naish, T. R., Levy, R. H., Fogwill, C. J., and Gasson, E. G.: The multi-millennial Antarctic commitment  
540 to future sea-level rise, *Nature*, 526, 421–425, 2015.

Hansen, M. B., Scheck-Wenderoth, M., Hübscher, C., Lykke-Andersen, H., Dehghani, A., Hell, B., and Gajewski, D.: Basin evolution of the northern part of the northeast German Basin—Insights from a 3D structural model, *Tectonophysics*, 437, 1–16, 2007.

Haq, B. U., Hardenbol, J., and Vail, P. R.: Chronology of fluctuating sea levels since the Triassic, *Science*, 235, 1156–1167, 1987.

Hayes, D. and Frakes, L.: Initial Reports of the Deep Sea Drilling Project 28, 1975.

545 Haywood, A. M., Valdes, P. J., Aze, T., Barlow, N., Burke, A., Dolan, A. M., Von Der Heydt, A., Hill, D. J., Jamieson, S., Otto-Bliesner, B. L., et al.: What can Palaeoclimate Modelling do for you?, *Earth Systems and Environment*, 3, 1–18, 2019.

Herold, N., Seton, M., Müller, R., You, Y., and Huber, M.: Middle Miocene tectonic boundary conditions for use in climate models, *Geochemistry, Geophysics, Geosystems*, 9, 2008.

Hochmuth, K., Gohl, K., Leitchenkov, G., Sauermilch, I., Whittaker, J. M., Uenzelmann-Neben, G., Davy, B., and De Santis, L.: The evolving  
550 paleobathymetry of the circum-Antarctic Southern Ocean since 34 Ma: A key to understanding past cryosphere-ocean developments, *Geochemistry, Geophysics, Geosystems*, 21, e2020GC009122, 2020.

Hoggard, M., White, N., and Al-Attar, D.: Global dynamic topography observations reveal limited influence of large-scale mantle flow, *Nature Geoscience*, 9, 456–463, 2016.

Hölzel, M., Faber, R., and Wägreich, M.: DeCompactionTool: Software for subsidence analysis including statistical error quantification,  
555 *Computers & geosciences*, 34, 1454–1460, 2008.

IPCC: Climate Change 2013: The Physical Science Basis. Contribution of Working Group I to the Fifth Assessment Report of the Intergovernmental Panel on Climate Change - Summary for policymakers, <https://doi.org/10.1017/CBO9781107415324.004>, 2013.

IPCC: IPCC Special Report on the Ocean and Cryosphere in a Changing Climate: Summary for Policymakers, 2019.

Jarvis, G. T. and McKenzie, D. P.: Sedimentary basin formation with finite extension rates, *Earth and Planetary science letters*, 48, 42–52,  
560 1980.

- Jha, S., Harry, D. L., and Schutt, D. L.: Toolbox for Analysis of Flexural Isostasy (TAFI)—A MATLAB toolbox for modeling flexural deformation of the lithosphere, *Geosphere*, 13, 1555–1565, 2017.
- Kirschner, J. P., Kominz, M. A., and Mwakanyamale, K. E.: Quantifying extension of passive margins: Implications for sea level change, *Tectonics*, 29, 2010.
- 565 Kominz, M. A., Patterson, K., and Odette, D.: Lithology dependence of porosity in slope and deep marine sediments, *Journal of Sedimentary Research*, 81, 730–742, 2011.
- Kusznir, N. J., Roberts, A. M., and Morley, C. K.: Forward and reverse modelling of rift basin formation, Geological Society, London, Special Publications, 80, 33–56, 1995.
- Lee, E. Y., Novotny, J., and Wagreich, M.: BasinVis 1.0: A MATLAB®-based program for sedimentary basin subsidence analysis and  
570 visualization, *Computers & Geosciences*, 91, 119–127, 2016.
- Lee, E. Y., Novotny, J., and Wagreich, M.: Compaction trend estimation and applications to sedimentary basin reconstruction (BasinVis 2.0), *Applied Computing and Geosciences*, 5, 100 015, 2020.
- MATLAB: version 9.9 (R2019b), The MathWorks Inc., Natick, Massachusetts, R2019b.
- McKenzie, D.: Some remarks on the development of sedimentary basins, *Earth and Planetary Science Letters*, 40, 25–32, 1978.
- 575 Miller, K. G., Browning, J. V., Schmelz, W. J., Kopp, R. E., Mountain, G. S., and Wright, J. D.: Cenozoic sea-level and cryospheric evolution from deep-sea geochemical and continental margin records, *Science advances*, 6, eaaz1346, 2020.
- Milne, G. A. and Mitrovica, J. X.: Searching for eustasy in deglacial sea-level histories, *Quaternary Science Reviews*, 27, 2292–2302, 2008.
- Müller, R., Hassan, R., Gurnis, M., Flament, N., and Williams, S. E.: Dynamic topography of passive continental margins and their hinterlands since the Cretaceous, *Gondwana Research*, 53, 225–251, 2018a.
- 580 Müller, R. D., Cannon, J., Williams, S., and Dutkiewicz, A.: PyBacktrack 1.0: A tool for reconstructing paleobathymetry on oceanic and continental crust, *Geochemistry, Geophysics, Geosystems*, 19, 1898–1909, 2018b.
- Müller, R. D., Zahirovic, S., Williams, S. E., Cannon, J. and Seton, M., Bower, D. J., Tetley, M. G., Heine, C., Le Breton, E., Liu, S., et al.: A global plate model including lithospheric deformation along major rifts and orogens since the Triassic, *Tectonics*, 38, 1884–1907, 2019.
- Noble, T., Rohling, E., Aitken, A. R. A., Bostock, H. C., Chase, Z., Gomez, N., Jong, L. M., King, M. A., Mackintosh, A. N., McCor-  
585 mack, F., et al.: The Sensitivity of the Antarctic Ice Sheet to a Changing Climate: Past, Present, and Future, *Reviews of Geophysics*, 58, e2019RG000 663, 2020.
- Otto-Bliesner, B. L., Jahn, A., Feng, R., Brady, E. C., Hu, A., and Löffverström, M.: Amplified North Atlantic warming in the late Pliocene by changes in Arctic gateways, *Geophysical Research Letters*, 44, 957–964, 2017.
- Paxman, G. J., Jamieson, S. S., Hochmuth, K., Gohl, K., Bentley, M. J., Leitchenkov, G., and Ferraccioli, F.: Reconstructions of Antarctic  
590 topography since the Eocene–Oligocene boundary, *Palaeogeography, palaeoclimatology, palaeoecology*, 535, 109 346, 2019.
- Paxman, G. J., Gasson, E. G., Jamieson, S. S., Bentley, M. J., and Ferraccioli, F.: Long-Term Increase in Antarctic Ice Sheet Vulnerability Driven by Bed Topography Evolution, *Geophysical Research Letters*, 47, e2020GL090 003, 2020.
- Reerink, T. J., Jan Van De Berg, W., and Van De Wal, R. S. W.: OBLIMAP 2.0: a fast climate model-ice sheet model coupler including online embeddable mapping routines, *Geoscientific Model Development*, 9, 4111–4132, 2016.
- 595 Riahi, K., van Vuuren, D. P., Kriegler, E., Edmonds, J., O’Neill, B. C., Fujimori, S., Bauer, N., Calvin, K., Dellink, R., Fricko, O., Lutz, W., Popp, A., Cuaresma, J. C., KC, S., Leimbach, M., Jiang, L., Kram, T., Rao, S., Emmerling, J., Ebi, K., Hasegawa, T., Havlik, P., Humpenöder, F., Da Silva, L. A., Smith, S., Stehfest, E., Bosetti, V., Eom, J., Gernaat, D., Masui, T., Rogelj, J., Stre-  
fler, J., Drouet, L., Krey, V., Luderer, G., Harmsen, M., Takahashi, K., Baumstark, L., Doelman, J. C., Kainuma, M., Klimont,



- Z., Marangoni, G., Lotze-Campen, H., Obersteiner, M., Tabeau, A., and Tavoni, M.: The Shared Socioeconomic Pathways and their energy, land use, and greenhouse gas emissions implications: An overview, *Global Environmental Change*, 42, 153 – 168, <https://doi.org/https://doi.org/10.1016/j.gloenvcha.2016.05.009>, 2017.
- Roberts, A., Corfield, R., Matthews, S., Kuszniir, N., Hooper, R., and Gjeldvik, G.: Structural development and palaeobathymetry at the Norwegian Atlantic margin: revealed by 3D flexural-backstripping, in: 6th Petroleum Geology Conference: North West Europe and Global Perspectives, London, Abstracts, vol. 46, 2003.
- Roberts, A. M., Kuszniir, N. J., Yielding, G., and Styles, P.: 2D flexural backstripping of extensional basins; the need for a sideways glance, *Petroleum Geoscience*, 4, 327–338, 1998.
- Roberts, A. M., Alvey, A. D., and Kuszniir, N. J.: Crustal structure and heat-flow history in the UK Rockall Basin, derived from backstripping and gravity-inversion analysis, *Petroleum Geoscience*, 25, 131–150, 2019.
- Scheck, M., Bayer, U., and Lewerenz, B.: Salt redistribution during extension and inversion inferred from 3D backstripping, *Tectonophysics*, 373, 55–73, 2003.
- Sclater, J. G. and Christie, P. A.: Continental stretching: An explanation of the post-Mid-Cretaceous subsidence of the central North Sea Basin, *Journal of Geophysical Research: Solid Earth*, 85, 3711–3739, 1980.
- Siddoway, C. S., Baldwin, S. L., Fitzgerald, P. G., Fanning, C. M., and Luyendyk, B. P.: Ross Sea mylonites and the timing of intracontinental extension within the West Antarctic rift system, *Geology*, 32, 57–60, 2004.
- Smallwood, J. R.: Back-stripped 3D seismic data: A new tool applied to testing sill emplacement models, *Petroleum Geoscience*, 15, 259–268, 2009.
- Spada, G. and Melini, D.: SELEN 4 (SELEN version 4.0): a Fortran program for solving the gravitationally and topographically self-consistent sea-level equation in glacial isostatic adjustment modeling, *Geoscientific Model Development*, 12, 5055–5075, 2019.
- Steckler, M. and Watts, A.: Subsidence of the Atlantic-type continental margin off New York, *Earth and Planetary Science Letters*, 41, 1–13, 1978.
- Steinberg, J., Roberts, A., Kuszniir, N., Schafer, K., and Karcz, Z.: Crustal structure and post-rift evolution of the Levant Basin, *Marine and Petroleum Geology*, 96, 522–543, 2018.
- Stock, J. and Cande, S.: Tectonic history of Antarctic seafloor in the Australia-New Zealand-South Pacific sector: Implications for Antarctic continental tectonics, *Royal Society of New Zealand bulletin*, pp. 251–259, 2002.
- Straume, E. O., Gaina, C., Medvedev, S., and Nisancioglu, K. H.: Global Cenozoic Paleobathymetry with a focus on the Northern Hemisphere Oceanic Gateways, *Gondwana Research*, 2020.
- Tamisiea, M., Mitrovica, J., Milne, G., and Davis, J.: Global geoid and sea level changes due to present-day ice mass fluctuations, *Journal of Geophysical Research: Solid Earth*, 106, 30 849–30 863, 2001.
- Turcotte, D. L. and Schubert, G.: *Geodynamics*, Cambridge University Press, 2 edn., <https://doi.org/10.1017/CBO9780511807442>, 2002.
- Wangen, M.: *Physical Principles of Sedimentary Basin Analysis*, Cambridge University Press, <https://doi.org/10.1017/CBO9780511711824>, 2010.
- Wickert, A.: Crustal structure and post-rift evolution of the Levant Basin, *Geoscientific Model Development*, 9, 997–1017, <https://doi.org/10.5194/gmd-9-997-2016>, 2016.
- Wienecke, S., Braitenberg, C., and Götze, H.-J.: A new analytical solution estimating the flexural rigidity in the Central Andes, *Geophysical Journal International*, 169, 789–794, 2007.

Zhang, Y. G., Pagani, M., Liu, Z., Bohaty, S. M., and DeConto, R.: A 40-million-year history of atmospheric CO<sub>2</sub>, *Philosophical Transactions of the Royal Society A: Mathematical, Physical and Engineering Sciences*, 371, 20130096, 2013.

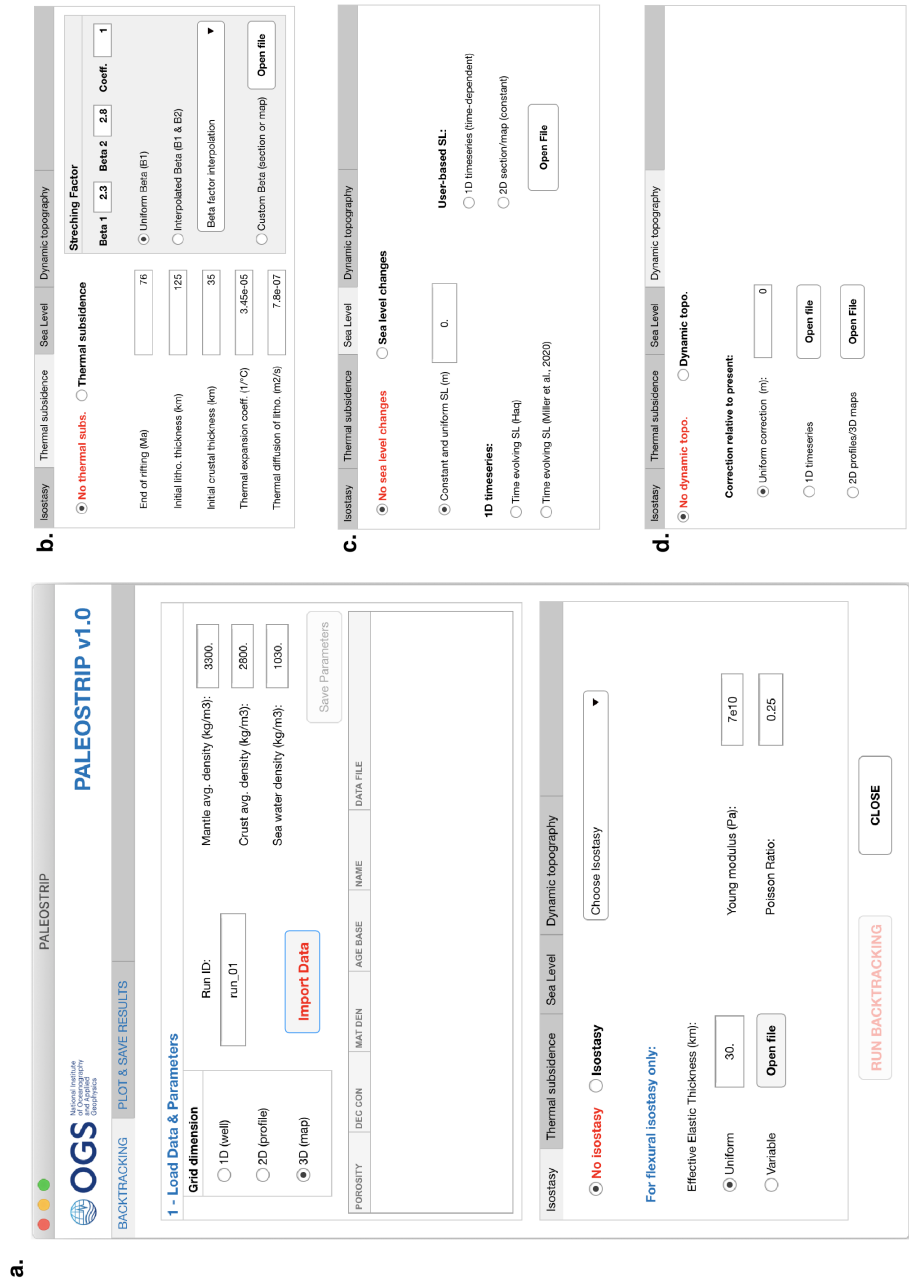


**Figure 1.** PALEOSTRIP Application GUI: a. Main PALEOSTRIP GUI; b. tab interface to set thermal subsidence (bottom of main GUI); c. tab interface to set Sea Level corrections; d. tab interface to set Dynamic topography correction.

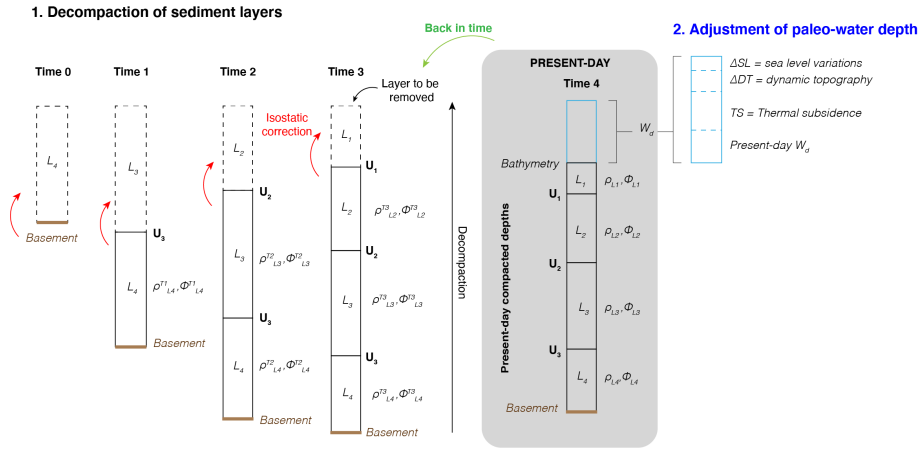


**Figure 2.** Backtracking procedure: sediment layers  $L$  are separated by well-defined seismic or lithological unconformities  $U$ . All the sediment layers have different lithological properties defined by their porosity  $\phi$  and density  $\rho$ . Those two properties changes during the decompaction process, departing from present-day depth of sediment layers, as buried sediments are unloaded from the upper sediment layers (isostatic correction). The water depth at each time step is calculated using time-varying thermal subsidence model (Eq. 3).

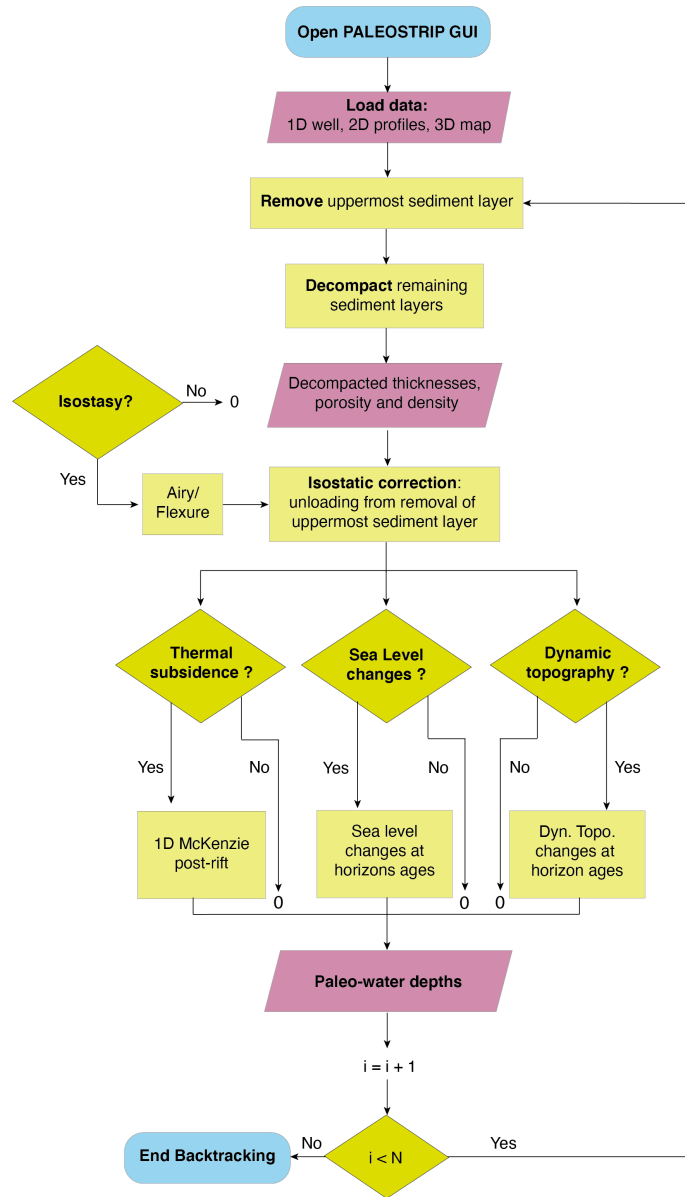
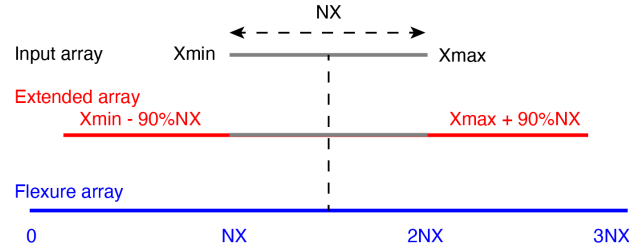


**Figure 3.** Workflow of the code implemented in PALEOSTRIP illustrating the various steps of computation according to selected options in the GUI.  $N$  sediment layers are decompacted during the backtracking procedure. Smooth blue rectangles correspond to start and end of the backtracking run. Light red parallelograms indicate input and output data. Light green rectangles are intermediate steps in the backtracking computation. Green diamonds correspond to options selected by the user in the GUI. If isostasy, or thermal subsidence, or sea level changes, or dynamic topography are switched off, the corresponding correction equals zero.

**a. 2D array expansion for flexural isostasy**



**b. 3D grid interpolation for flexural isostasy**

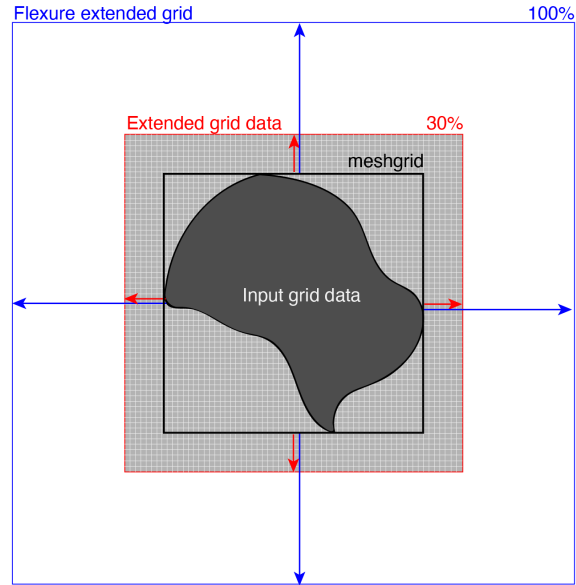


**Figure 4.** 2D and 3D domain expansion for computation of flexural isostasy: a. In case of 2D vertical sections, input data are extended with the edges values for 90% of the initial total array length (NX). This extended array is placed at the centered of a null array three times larger than the initial input data array.; b. In case of 3D maps, input data are extrapolated with a nearest neighbor algorithm on a mesh grid (black) to obtain a structured squared grid if the initial data are given on an irregular polygon. This mesh grid is extended by 30% on all edges (red) and is placed at the centered of a grid twice as large as the mesh grid obtained from initial input data (blue).

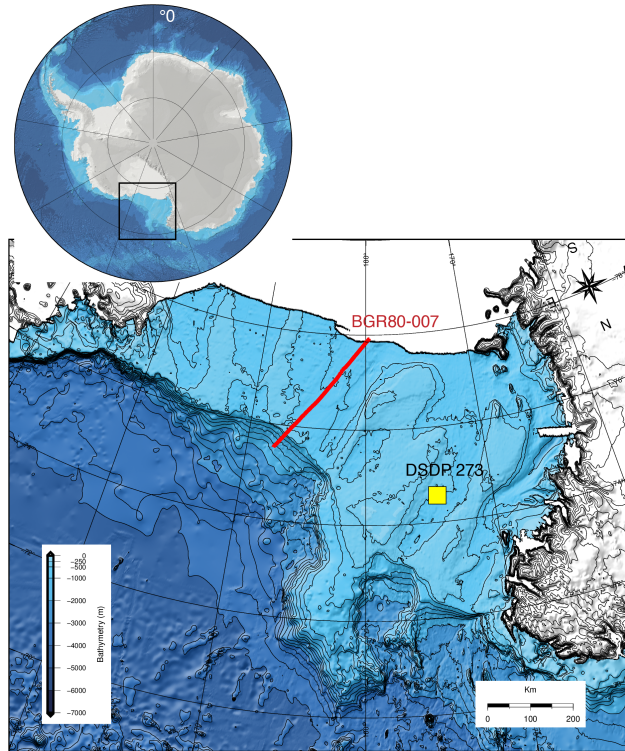


**Figure 5.** Close-up of the Ross Sea bathymetry from IBCSO (Arndt et al., 2013) and its location in Antarctica. Most of the ice-free bathymetry is backtracked as a case studies below. The BGR80-007 2D marine seismic transect used for validation is indicated with a red line and the DSDP 273 site location, backtracked in the case studies below, is indicated with a yellow square.

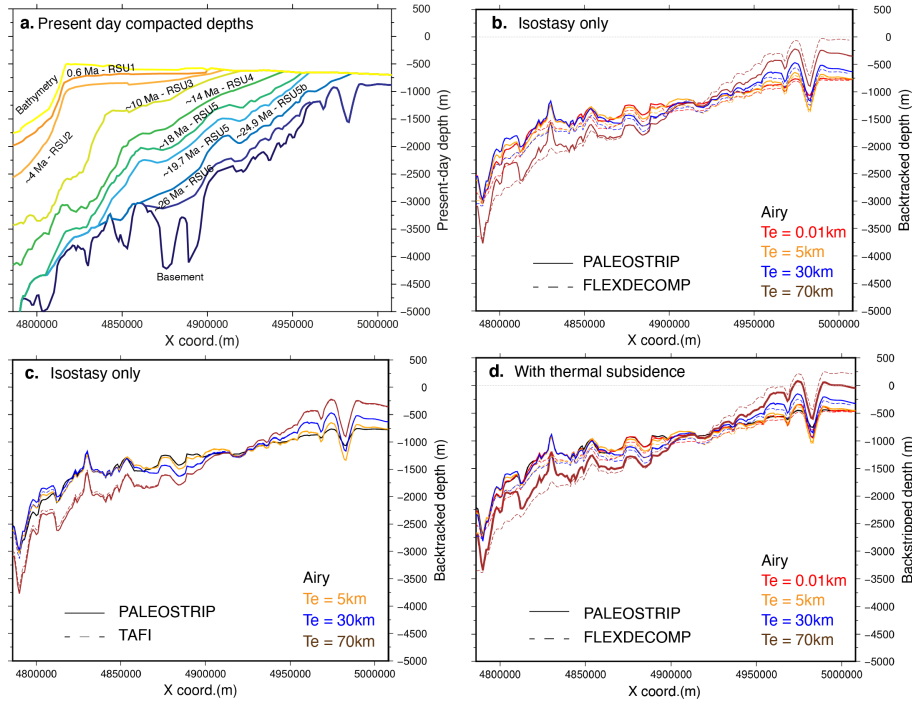


**Figure 6.** 2D transect BGR80-007 case study: a. Input present-day compacted depths (m) of bathymetry (yellow), and the nine seismic unconformities, amongst which, the mid-Miocene Ross Sea Unconformity 4 (RSU4) and basement (thick blue line). Layout is from PALEOSTRIP Plot GUI. Comparison of backtracked basement depths for different but spatially uniform lithospheric elastic thicknesses ( $T_e$ ): b. between PALEOSTRIP finite difference isostasy and Flex-Decomp (Kusznir et al., 1995) Fast Fourier Transform (wavenumber-based) isostasy model; c. between PALEOSTRIP finite difference isostasy and TAFI (Jha et al., 2017) Green's function spectral isostasy model; d. Same as b. but accounting for thermal subsidence correction using an age of Rift = 85 Ma and a uniform  $\beta = 2$ .



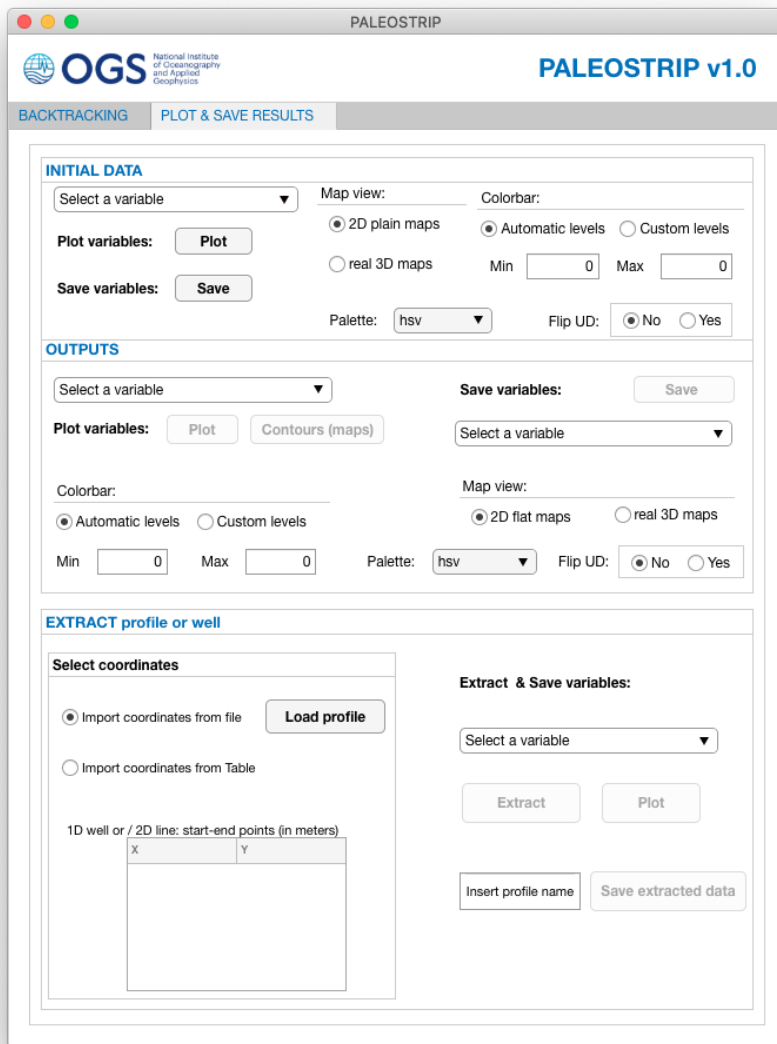


**Figure 7.** PALEOSTRIP Application GUI: Plot & Save Results interface.

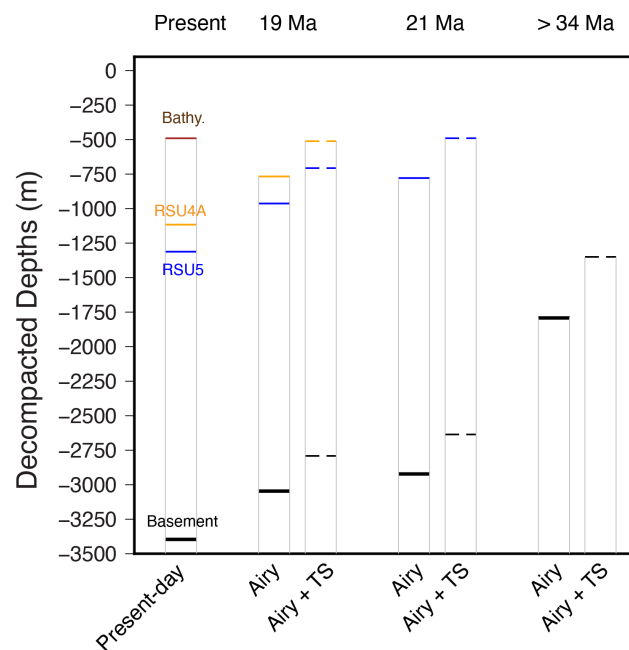


**Figure 8.** Backtracking steps for Western Ross Sea DSDP 273 well site. For present-day: present-day depths of basement (black), Ross Sea unconformity 5 ( blue), Ross Sea Unconformity 4A (orange) and bathymetry (brown); at time of RSU4A (19 Ma), at time of RSU5 (21 Ma) and at time before glacial sediment deposition (> 34 Ma). For each time step, two backtracking are shown, one accounting for Airy isostatic correction only, and one accounting for Airy isostatic correction and thermal subsidence (dashed). Table 1 in Appendix A.

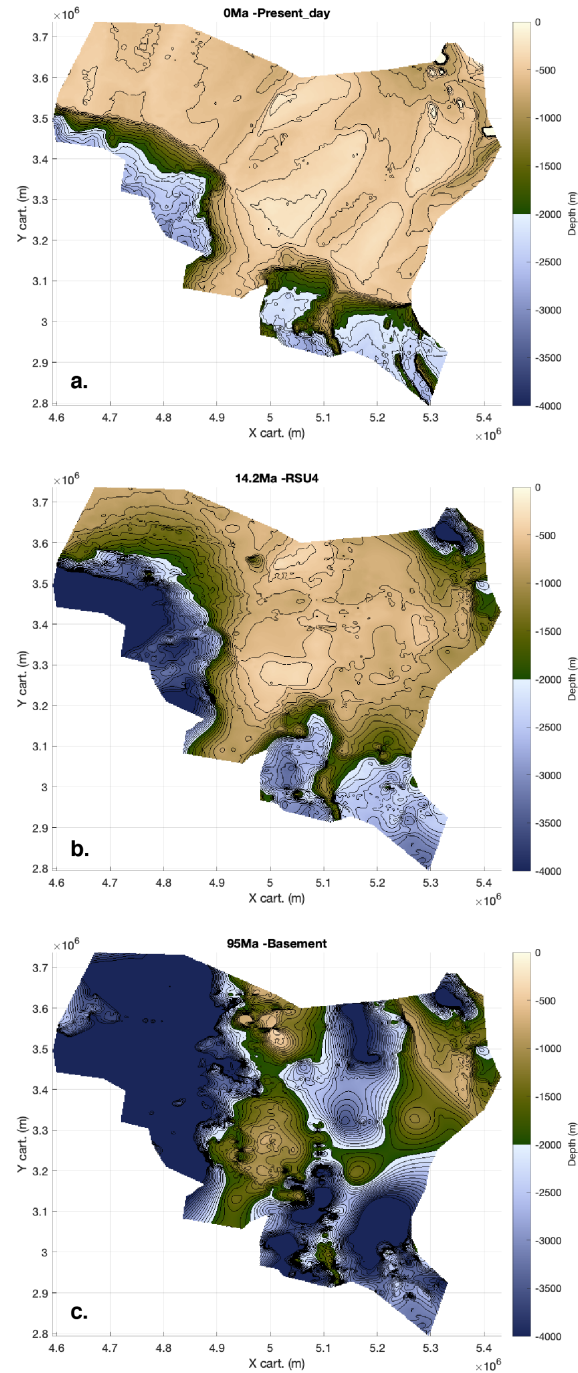
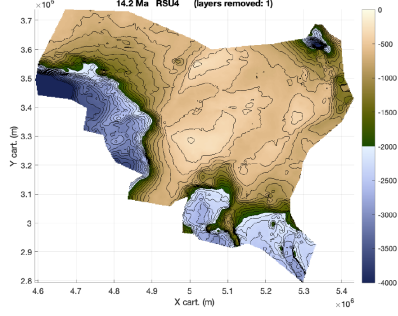
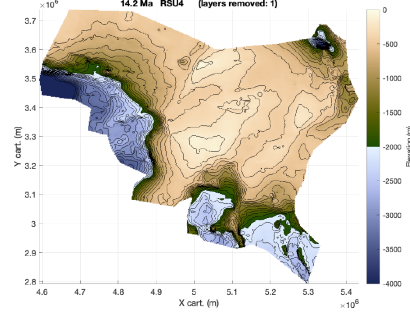


**Figure 9.** Initial input present-day depths (m): a. bathymetry, b. mid-Miocene unconformity RSU4 and c. basement both from ANTOSTRAT atlas (Brancolini et al., 1995). Layout is from PALEOSTRIP plotting GUI and the colorscale is the default colorscale implemented within PALEOSTRIP. Colorscale has been saturated below -4000 meters and above 200 meters for the need of this figure: the maximum depth of the basement reaches -10 km and would have largely damped the other bathymetric changes occurring at shallower depths in panels a) and b). The island located on the uppermost right corner is the only location with elevation above sea level. Note that the color scale is color-blind friendly and is from Crameri et al. (2020). PALEOSTRIP has implemented 12 different color scales, 9 out of 12 are color-blind friendly.

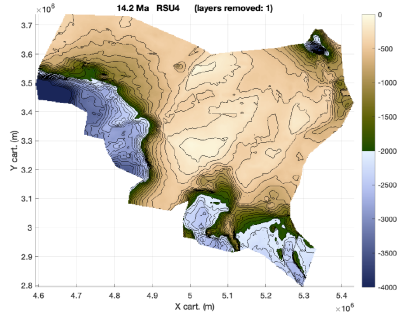
a. Airy only



b. Airy + Thermal subsidence



c. Airy + Thermal subsidence + Sea level



d. Airy + Thermal subs. + Sea level + Dynamic Topo.

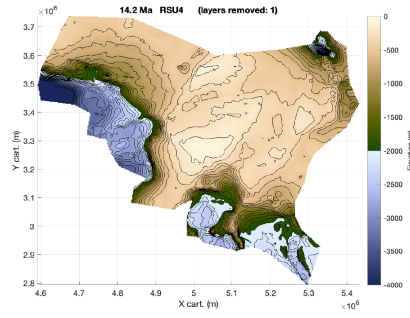
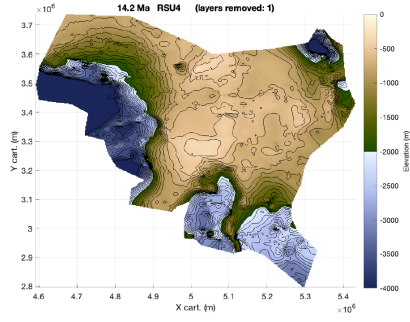


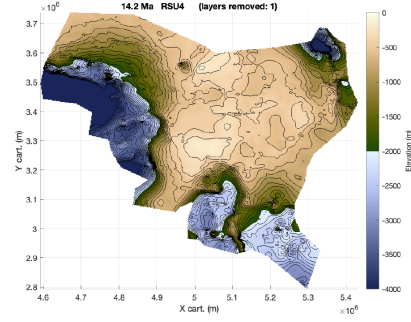
**Figure 10.** Backtracked Mid-Miocene bathymetries at about 14 Ma: a. corrected only for Airy isostasy; b. same as a. but including thermal subsidence correction with a spatially uniform  $\beta = 2.1$  and the end of rifting sets at 76 Ma; c. same as b. but including eustatic sea level correction based on Miller et al. (2020)  $\delta^{18}O$ -derived reconstruction; d. same as c. but including dynamic topography correction based on Müller et al. (2018a) geodynamical model M1 (following Hochmuth et al., 2020). Layout is from PALEOSTRIP plotting GUI and the colorscale is the default colorscale implemented within PALEOSTRIP and has been saturated below -4000 meters and above 200 meters for the need of this figure. The island located on the uppermost right corner is the only location with elevation above sea level. Note that the color scale is color-blind friendly and is from Crameri et al. (2020). PALEOSTRIP has implemented 12 different color scales, 9 out of 12 are color-blind friendly

. For all parameters used in those example see Table ??

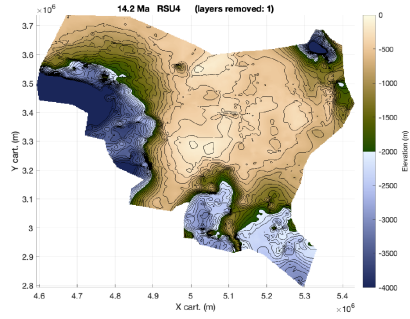
a. Flexure only



b. Flexure + Thermal subsidence



c. Flexure + Thermal subsidence + Sea level



d. Flex. + Thermal subs. + Sea level + Dynamic Topo.

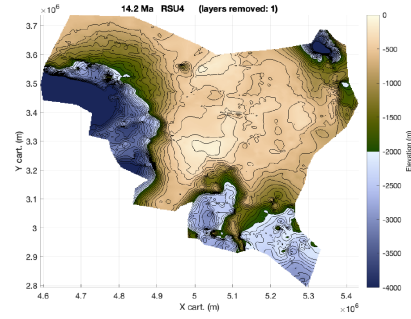


**Figure 11.** Backtracked Mid-Miocene bathymetries at about 14 Ma. Same as Fig. 10 but using flexural isostasy with spatially variable lithospheric effective elastic thickness from Chen et al. (2018). Layout is from PALEOSTRIP plotting GUI and the colorscale is the default colorscale implemented within PALEOSTRIP and has been saturated below -4000 meters and above 200 meters for the need of this figure. The island located on the uppermost right corner is the only location with elevation above sea level. Note that the color scale is color-blind friendly and is from Crameri et al. (2020). PALEOSTRIP has implemented 12 different color scales, 9 out of 12 are color-blind friendly. For all parameters used in those example see Table 1 in Appendix A.

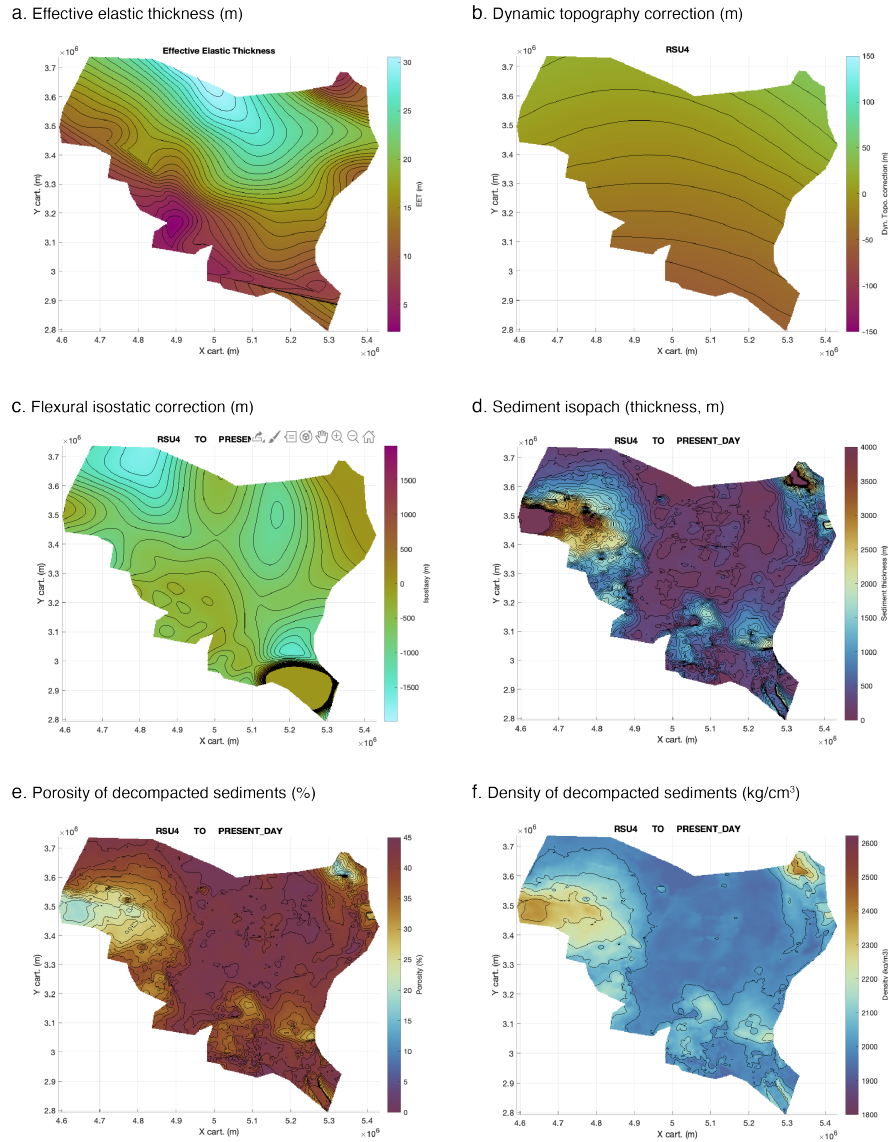


**Figure A1.** Example of input data and related backtracked sediment variables at Mid-Miocene: a. spatially variable lithospheric elastic thickness (Chen et al., 2018); b. Dynamic topography correction (Müller et al., 2018b). Both a. and b. are user-provided input to PALEOSTRIP; c. Flexural isostatic correction calculated using a.; d. Decompacted isopach (m); e. Decompacted porosity (%); f. Decompacted density ( $\text{kg}/\text{cm}^3$ ). Note that the color scale is color-blind friendly and is from Crameri et al. (2020). PALEOSTRIP has implemented 12 different color scales, 9 out of 12 are color-blind friendly.

**Table 1.** Physical parameters values used in the case studies.

<b>Isostasy:</b>	
Young modulus (Pa)	7e10
Poisson Ratio	0.25
<b>Thermal Subsidence:</b>	
End of rifting (Ma)	76
Initial lithospheric thickness (km)	125
Initial crustal thickness (km)	35
Thermal expansion coefficient (1/deg C)	3.45e-05
Thermal diffusion of lithosphere (m <sup>2</sup> /s)	3.45e-05
Streching Factor	2.1
<b>Sea Level correction:</b>	
1D timeseries	Miller et al. (2020)
<b>Dynamic Topography:</b>	
3D maps	time-evolving and spatially varying Müller et al. (2018b)